

Algorithms for uniform particle initialization in domains with complex boundaries

Pawan Negi^{a,*}, Prabhu Ramachandran^a

^a*Department of Aerospace Engineering, Indian Institute of Technology Bombay, Powai, Mumbai 400076*

Abstract

Accurate mesh-free simulation of fluid flows involving complex boundaries requires that the boundaries be captured accurately in terms of particles. In the context of incompressible/weakly-compressible fluid flow, the SPH method is more accurate when the particle distribution is uniform. Hence, for the time accurate simulation of flow in the presence of complex boundaries, one must have both an accurate boundary discretization as well as a uniform distribution of particles to initialize the simulation. This process of obtaining an initial uniform distribution of particles is called “particle packing”. In this paper, various particle packing algorithms present in the literature are implemented and compared. An improved SPH-based algorithm is proposed which produces uniform particle distributions of both the fluid and solid domains in two and three dimensions. Some challenging geometries are constructed to demonstrate the accuracy of the new algorithm. The implementation of the algorithm is open source and the manuscript is fully reproducible.

Keywords: Particle packing, complex geometry, pre-processing, smoothed particle hydrodynamics

Program summary

Program title: SPHGeom

*Corresponding author

Email addresses: `pawan.n@aero.iitb.ac.in` (Pawan Negi),
`prabhu@aero.iitb.ac.in` (Prabhu Ramachandran)

Licensing provisions: BSD 3-Clause

Programming language: Python

External routines/libraries: PySPH (<https://github.com/pypr/pysph>), matplotlib (<https://pypi.org/project/matplotlib/>), automan (<https://pypi.org/project/automan/>), ParaView(<https://www.paraview.org/download/>).

Nature of problem: Particle methods require that complex geometry be represented accurately when discretized with particles. The particles should be uniformly distributed inside, outside, and on the surface of the geometry. A particle packing algorithm is proposed to achieve this. For a fluid flow past a solid body, the code generates a set of solid particles inside and on the surface surrounded by fluid particles such that the density is approximately constant. These particles can be placed anywhere in the main simulation.

Solution method: An SPH-based algorithm is proposed where the number density gradient, a repulsion force, and a damping force are used to move particles. Particles are constrained near the boundary to move along the surface. Particles are iteratively projected onto the boundary surface. Once a desired distribution of particles is achieved, the particles are separated into interior and exterior particles using the boundary information. This may be used directly as an input for particle-based simulation.

Additional comments: The source code for this repository can be found at https://gitlab.com/pypr/sph_geom.

1. Introduction

Smoothed Particle Hydrodynamics (SPH) is a mesh-free numerical method used for the simulation of continuum mechanics problems. It was first proposed by Gingold and Monaghan [1] and Lucy [2]. Unlike mesh-based methods, the SPH method discretizes the domain into particles that carry physical properties. The SPH method has been employed to study a wide variety of problems. A comprehensive list of schemes can be found in Liu and Liu [3], Violeau [4], and Ye et al. [5].

The SPH method approximates functions and derivatives by using a convolution with a smooth kernel function

$$f(\mathbf{x}) = \int_{\Omega} f(\tilde{\mathbf{x}})W(\mathbf{x} - \tilde{\mathbf{x}}, h)d\tilde{\mathbf{x}} + O(h^2), \quad (1)$$

where Ω is the domain, $W(\mathbf{x} - \tilde{\mathbf{x}}, h)$ is a compact kernel function with properties described in [6] and h is the support radius of the kernel. The domain

is discretized into particles carrying the required properties. This integral is then discretized as

$$f(\mathbf{x}) \approx \sum_j f(\mathbf{x}_j) W(\mathbf{x} - \mathbf{x}_j, h) \frac{m_j}{\rho_j}, \quad (2)$$

where \mathbf{x}_j is the position of the j^{th} particle and $V_j = \frac{m_j}{\rho_j}$ is the volume associated with the particle with mass m_j and density ρ_j . This approximation is most accurate when the underlying particle distribution is uniform [7, 8]. For example, the particles could be placed on a uniform Cartesian mesh with constant spacing. However, the SPH method is Lagrangian and the particles move with the local velocity field. Many recent developments in SPH involve the use of Particle Shifting Techniques (PST)[9, 10, 11] which shift the particles towards a uniform distribution. Thus, it is important to have a uniform distribution of particles.

Consider the case of the two-dimensional flow past a simple non-Cartesian solid shape like a circular cylinder. The fluid flow occurs outside of the cylinder. In the SPH method, the fluid is discretized using (fluid) particles. The circular cylinder is also discretized with (solid) particles. These solid particles are not merely on the surface of the cylinder but also on its interior for accuracy of the method. When the simulation starts, we require a uniform distribution of both fluid and solid particles which capture the geometry accurately. Clearly, one cannot use a Cartesian mesh of particles and still describe the cylinder surface accurately.

We must therefore define the term “uniform” distribution of particles in the context of the SPH method. This has been discussed by Colagrossi et al. [12] and Litvinov et al. [13]. They explain that a non-uniform distribution would generate a spurious force among the particles leading to a “resettlement” of their spatial distribution.

As discussed in [12], for particles having the same mass and density, we can estimate the non-uniformity using either,

$$\Gamma_i = \sum_j W(\mathbf{x}_i - \mathbf{x}_j, h) \frac{m_j}{\rho_j}, \quad (3)$$

where \mathbf{x}_i refers to the i^{th} particle or

$$\nabla \Gamma_i = \sum_j \nabla W(\mathbf{x}_i - \mathbf{x}_j, h) \frac{m_j}{\rho_j}. \quad (4)$$

where ∇W is the gradient of the kernel function with respect to \mathbf{x}_i . If $\Gamma_i = 1$ or $\nabla\Gamma_i = 0$, then the particle distribution may be considered uniform. For example, for particles placed on an infinite Cartesian mesh $\Gamma_i \approx 1$, $\nabla\Gamma_i \approx 0$ for all particles. In this paper, particle distributions that satisfy this requirement are referred to as uniform, homogeneous, or regular distributions interchangeably. The term “particle packing” is used in the literature as the process of generating such a homogeneous distribution of particles.

There are many higher-order SPH schemes like [14, 15, 16, 17] which employ corrected kernel functions such that $\Gamma_i = 1$ and $\nabla\Gamma_i = 0$ by construction regardless of the underlying particle distribution. In such cases it may be argued that there is no requirement for a uniform/homogeneous distribution of particles. However, these methods do not always ensure the conservation of linear and angular momentum. On the other hand, the uncorrected kernels when used with a suitable formulation do conserve linear and angular momentum as discussed in [17]. Therefore, even with a higher-order SPH method, it is usually desirable to have a reasonably uniform distribution of fluid and solid particles to improve conservation [8].

Many problems involving complex geometries have been solved in the SPH literature. For example, the flow around blades of mixing devices [18] and industrial automotive problems [19]. In order to simulate such problems, the initial particle distribution must capture important features of the geometry accurately while maintaining a uniform spatial distribution.

There have been some earlier attempts to do this in the context of SPH. Colagrossi et al. [12] devised a particle packing algorithm which uses the kernel gradient to distribute the particles in two-dimensions around a solid body such that the simulation starts smoothly. In order to generate the two-dimensional solid, the method proposed by Marrone et al. [20] was employed. The method constructs solid boundaries using piecewise linear curves (PLC). These are translated along the normal and discretized into equispaced particles according to the desired particle spacing, Δs , up to the required number of layers. Xiao et al. [21] proposed an algorithm to divide the two-dimensional domain of interest into square-shaped sub-domains. The sub-domains having an area equal to the desired area (Δs^2) are directly converted to particles. Other particles near the boundary are given partial mass iteratively. None of these approaches consider three-dimensional geometries. Domínguez et al. [22] constructs geometries by clipping the grid with the boundary of the geometry, and this necessitates using a much higher resolution to capture the features better. Akinci et al. [23] proposed a scheme to place particles over

triangles of length greater than the particle spacing. This approach provides a good density distribution and has been employed to simulate flow for graphics applications in three dimensions. In a different context, Jiang et al. [24] used the SPH method for packing particles in order to sample blue noise. This method focuses on packing the particles inside and on the surface of the body. The method does not generate any particles outside the body. In order to obtain a uniform particle distribution, a kernel gradient along with a cohesive force proposed by Akinici et al. [23] is used. It balances the extra force on the particles near the surface.

In this paper, the methods proposed by Colagrossi et al. [12] and Jiang et al. [24] are implemented. The method of Jiang et al. [24] does not by default generate particles in the exterior of the boundary. A modification of the algorithm is proposed so that it generates the desired particles in the interior and exterior. A novel SPH-based method to construct two and three-dimensional geometries, at a given resolution, keeping the features of the geometry as detailed possible, is proposed. The following nomenclature is used henceforth to refer to the methods implemented:

- *Standard*: The geometry is created using the method proposed by Marone et al. [20] and particles are packed using the method proposed by Colagrossi et al. [12]. It must be noted that the method proposed in [20] is limited to two-dimensional geometries.
- *Coupled*: The interior (solid) and exterior (fluid) are created separately using the method proposed by Jiang et al. [24]. Once these converge, the interior and exterior interact using the method of [12].
- *Hybrid*: The proposed new method which combines features from the above two approaches.

The hybrid method uses the kernel gradient to move the particles as proposed by Colagrossi et al. [12] along with a strong repulsion force, which comes into effect only when two particles are closer than the particle spacing. The particles on the boundary are allowed to move over the surface only as done in [24]. Particles that are not on the boundary, are allowed to move in and out of the boundary surface. Particles are projected on the boundary which introduces disorder causing the other particles to adjust accordingly. It is important to note that the proposed algorithm can be applied in the context of any general-purpose SPH framework. This makes the approach

relatively easy to integrate into SPH codes. The present implementation uses the open-source PySPH framework [25, 26]. The particle distributions generated using the above methods are compared for different geometries. The accuracy of the proposed method is demonstrated by performing an SPH function and derivative approximation for a known function.

The paper is divided into four sections. The next section briefly discusses the SPH method. The section 3 describes the algorithms implemented in detail. In section 4, different geometries are constructed using the algorithms implemented. In the interest of reproducibility, the implementation of the algorithms is open source and all the results are fully reproducible.

2. Smoothed particle hydrodynamics

As discussed in the introduction, the SPH method approximates a function using a smooth, compact kernel, $W(\mathbf{x})$. Popular choices for the kernel in the SPH community are the Gaussian [6], splines [27] and the family of Wendland kernels [28]. In order to reproduce the given function with $O(h^2)$ accuracy, the kernel function must have

$$\int_{\Omega} W(\mathbf{x} - \tilde{\mathbf{x}}, h) d\tilde{\mathbf{x}} = 1, \text{ and } \int_{\Omega} \nabla W(\mathbf{x} - \tilde{\mathbf{x}}, h) d\tilde{\mathbf{x}} = \mathbf{0}. \quad (5)$$

In the continuous approximation, all of these kernel satisfy these properties [7]. In the SPH method, the domain is discretized using points each having mass m and density ρ . The discrete approximation of the density ρ and its gradient is given by

$$\rho_i = \sum_{j=1}^N m_j W_{ij} \text{ and } \nabla \rho_i = \sum_{j=1}^N m_j \nabla W_{ij}, \quad (6)$$

where $W_{ij} = W(x_i - x_j, h)$, m_j is the mass of i^{th} particle and N is the number of neighbors in the kernel support. We can see that if all particles have the same density $\rho_i = 1$, then, eq. (6) becomes the same as eq. (3) and eq. (4). We therefore assume that all particles have a unit density henceforth.

For a uniform distribution of particles, the value of $\Gamma_i = 1$ and $\nabla \Gamma_i = 0$ accurate to the order $O(h^2)$. Furthermore, as discussed in Kiara et al. [8], the kernel and its gradient can be corrected such that the condition in eq. (3) and eq. (4) are satisfied even for a non-uniform distribution of particles. However, using a corrected kernel introduces issues in momentum conservation when

the particles are non-uniform. Therefore, it is important to have a uniform particle distribution.

In the weakly compressible SPH scheme, the dynamics of the fluid flow is governed by

$$\frac{d\rho}{dt} = -\rho \nabla \cdot \mathbf{u}, \quad (7)$$

$$\frac{d\mathbf{u}}{dt} = -\frac{\nabla p}{\rho} + \nu \nabla^2 \mathbf{u}, \quad (8)$$

$$p = p(\rho, \rho_0, c_0) \quad (9)$$

where ρ , ν , p , \mathbf{u} are the density, kinematic viscosity, pressure and velocity of a discrete fluid particle respectively. ρ_0 and c_0 are the reference density and speed of sound. The derivatives can be approximated using various forms cf. [4]. In a simulation with a solid body, for example the flow past a cylinder, the solid particles are represented using classical dummy particles [29]. The use of a rectangular lattice would comply with the condition in eq. (6) however, the resulting boundary will be jagged. In order to produce a body conforming initial particle distribution such that the conditions in eq. (5) is satisfied, various particle packing algorithms are discussed in detail in the next section. We note that once the packing algorithm completes that there may be slight variations in the density of the order of around 2-3%. Colagrossi et al. [12] propose that the particle masses be changed so as to produce a constant density given the initial pressure field. This may be performed after the packing algorithm is complete if desired.

3. Particle packing algorithms

In this section, the proposed hybrid algorithm followed by other algorithms are discussed in detail.

3.1. Hybrid Algorithm

The schematic shown in fig. 1, depicts the different kinds of particles used in the proposed algorithm. In this figure, we consider the case of a cylinder surrounded by fluid. The dashed black line represents the surface of the cylinder (boundary surface) which we wish to capture accurately. We assume that this surface is discretized into a set of points called “boundary nodes”. The different kinds of entities shown in the figure are,

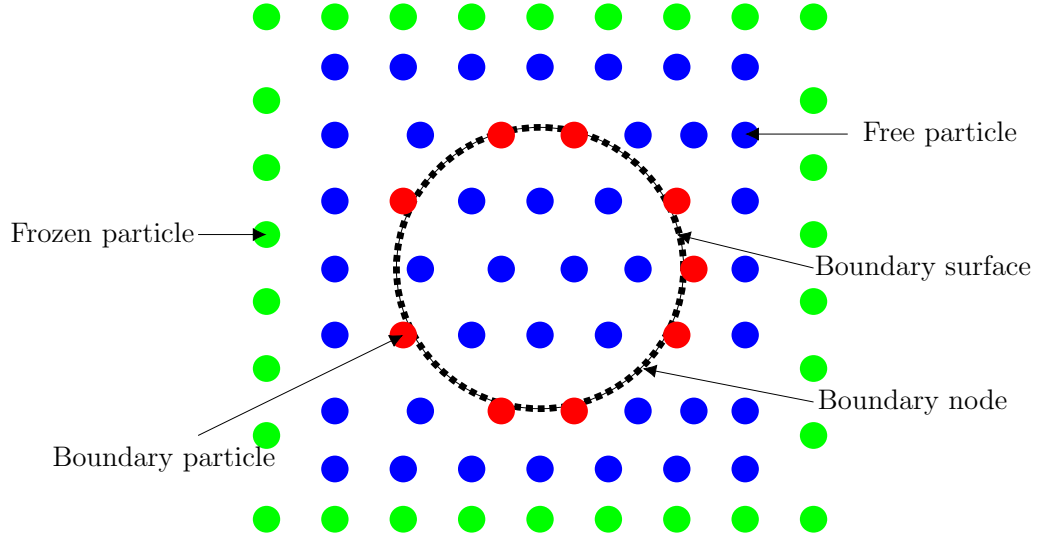


Figure 1: Schematic of the initial distribution of particles and the different kinds of particles.

- *Free particles*: These are particles arranged initially in a rectangular or hexagonal-packed pattern. Their motion is not constrained. These are depicted as blue circles.
- *Frozen particles*: These are a set of fixed classical dummy particles which surround the free particles in order to provide support to the kernel. These are depicted as green circles.
- *Boundary particles*: These particles are constrained to move along the “boundary surface” and are depicted as red circles.
- *Boundary surface*: The surface of the geometry that is discretized. It is represented by a set of fixed points, called “boundary nodes” which do not influence any other particles.
- *Boundary node*: These are points that discretize the boundary surface, they also store the local surface normals of the boundary surface. These are depicted as black dashes. We note that these are called nodes because they do not exert any forces on particles and only serve to provide information on the position and orientation of the boundary surface.

During the algorithm, free particles (blue) may be converted to boundary particles (red) if they are close to the boundary surface. Once the proposed algorithm completes, the red boundary particles must conform to the boundary represented by the dashed black line. The blue particles inside the dashed boundary will be considered as solid (dummy) particles and those outside as fluid particles.

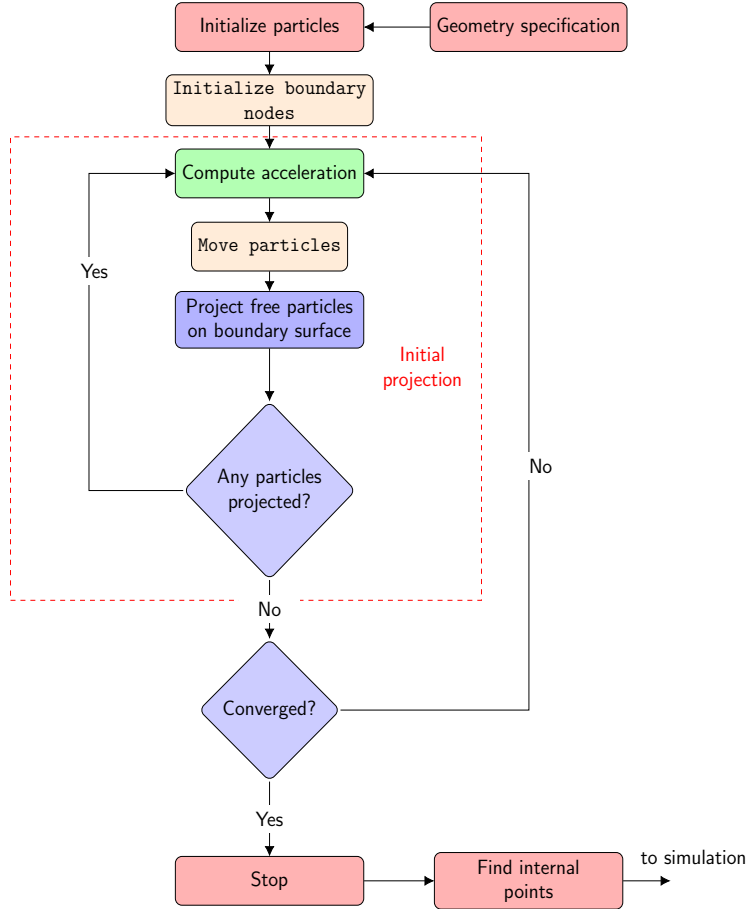


Figure 2: Flowchart of the particle packing algorithm. The box outlined in dashed red lines is the initial projection phase.

The overall flow of the algorithm is shown in fig. 2. The algorithm requires two inputs, the geometry information, and the desired particle spacing. These are to be provided by the user. Given the geometry surface, we first estimate the number of particles that should lie on this surface, N_s , using

the desired spacing of particles and either the length in 2D or the surface area in 3D.

Initially, the frozen particles are created on the periphery of the domain as shown in fig. 1 and placed on a rectangular lattice. Free particles are then placed inside this on a regular lattice. At this stage, no boundary particles are identified. The boundary nodes are initialized using the information provided by the user.

The acceleration on the free particles and any boundary particles (that are identified later) is computed using a local density gradient, and a repulsive force. This corresponds to the green block in fig. 2. The particles are moved using the computed accelerations. As the free particles move, they are converted to boundary particles if they are close enough to the boundary surface. They are then projected to the nearest point on the boundary surface. These boundary particles are constrained to move only along the boundary surface. The free particles are iteratively converted to boundary particles until no free particle is sufficiently close to the boundary.

During the initial projection phase (denoted by the red dashed line in the fig. 2), the particles are regularly projected onto the boundary surface. This is done until the number of boundary particles have reached N_s and remains there for a few consecutive iterations. The algorithm then proceeds to settle the particles into a uniform distribution until the displacement of the particles is less than a user-defined tolerance. This is denoted as the “Converged” block in fig. 2. Once convergence is attained, the boundary and free particles inside and outside the surface are packed as desired. Since the boundary surface is known, free particles can be easily identified as solid and fluid particles.

This packed collection of free and boundary particles may be placed into a larger regular mesh of particles for a simulation. For example, see fig. 3 where the dashed region is where the packed particles could be placed. The exterior of this region (shown in green) can be represented as a regular mesh of the same spacing. This approach is convenient to use in the context of fluid flow past solid bodies as done for internal flows [30] and free surface flows [31]. The algorithm described above is explained in detail in the subsequent sections.

3.1.1. Initialization of boundary nodes

The boundary nodes which represents the boundary surface are first initialized. In a two-dimensional domain, a set of points are required which discretize the boundary curve. The boundary curve may be parametrized

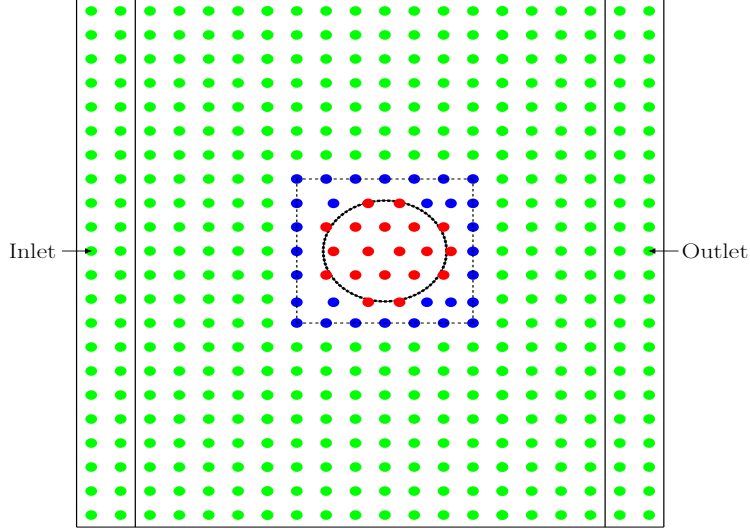


Figure 3: The preprocessed patch (dashed) of particles placed in the appropriate location of a typical simulation. The blue particles denote the free particles identified as fluid particles, the red represents the solid particles identified by the packing process. The green particles are generated from a fixed mesh of points.

by λ , and points on the curve may be specified as $\mathbf{x} = C(\lambda)$ and $\lambda \in [0, 1]$. This curve is discretized such that $\mathbf{x}_i = C(\lambda_i)$. The spacing between points must be such that $|\mathbf{x}_{i+1} - \mathbf{x}_i| < \Delta s$. The boundary node coordinates are initialized using these points. The outward normals n_x, n_y for any node i are calculated using

$$\begin{aligned} n_{x,i} &= 0.5 \left(\frac{y_{i+1} - y_i}{d_{i+1,i}} + \frac{y_i - y_{i-1}}{d_{i,i-1}} \right) \\ n_{y,i} &= -0.5 \left(\frac{x_{i+1} - x_i}{d_{i+1,i}} + \frac{x_i - x_{i-1}}{d_{i,i-1}} \right) \end{aligned} \quad (10)$$

where $d_{i,j}$ is the length of the segment joining node at (x_i, y_i) and (x_j, y_j) . The resulting normal is then normalized. The eq. (10) ensures that sharp corners of the curve have smooth normals. For a three-dimensional case, a triangulation of the surface with outward normals is necessary. The centroid of each triangle and its normal is used to initialize the boundary nodes.

In SPH, the actual boundary surface is exactly in between solid and fluid particles. Thus, both in two and three dimensions, given a particle spacing of Δs , the boundary nodes are shifted by $\Delta s/2$ inside the actual boundary to

correctly implement the solid boundary conditions as discussed in Marrone et al. [20]. In order to move the nodes inwards, the following translation is performed on each boundary node given by,

$$\mathbf{x} = \mathbf{x} - \frac{\Delta s}{2} \hat{\mathbf{n}}, \quad (11)$$

where, \mathbf{x} is the position of the node and $\hat{\mathbf{n}}$ is its unit normal pointing outwards. It must be noted that this is optional and one can provide a pre-shifted surface and avoid eq. (11).

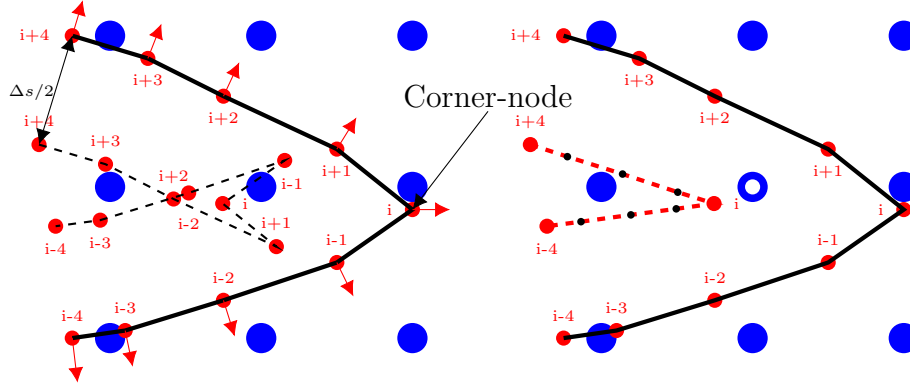


Figure 4: Shifting of the boundary near a sharp edged boundary. The boundary nodes are depicted in red with normals. On the left is the boundary surface after the initial shifting shown as black dashed lines. On the right is the final geometry after removal of the intersecting edges which are shown as dashed red lines. The annular blue free particle is the candidate to be placed on the corner and held fixed.

Care must be taken when there are sharp changes in the features of the geometry. Consider an airfoil trailing edge in fig. 4 shown as a black line. These sharp corners are marked as “corner nodes”, and in this case, it is the i^{th} node. When the nodes on this surface are shifted, the boundary surface tends to self-intersect itself. This is shown by the red nodes connected using a black dashed line. In order to remove the intersection of the boundary surface near the corner node, the points $i - 3$ to $i - 1$ are replaced by the points on the line joining $i - 4$ and i with equal spacing shown by black points. Similarly the points $i + 1$ to $i + 3$ are also replaced to lie along the line joining points i and $i + 4$. This results in a non-intersecting surface as shown by the red dashed line in the right side of fig. 4. Once the intersection is resolved, the nearest free particle near the corner node (annular blue particle) is placed

on it and converted to a *fixed boundary particle*. The position of these fixed boundary particles do not change in the entire simulation.

In the case of a three-dimensional object, one has to make sure that the surface does not intersect after applying eq. (11) or use a pre-shifted surface as an input.

3.1.2. Dynamics of the particles

In this section, the dynamics of particle regularization is discussed. Two forces are applied on the particles and together these regularize the particle distribution. The two forces are, a gradient due to particle disorder and a pure inter-particle repulsive force.

In the presence of a constant pressure field, p_b and no viscous effect, the momentum equation (eq. (8)), becomes

$$\frac{d\mathbf{u}}{dt} = -\frac{\nabla(1 \cdot p_b)}{\rho} = -\frac{p_b \nabla(1) + \nabla(p_b)}{\rho}. \quad (12)$$

When the term, $p_b \nabla(1)$, on the right hand side is discretized using the SPH method, we obtain $p_b \nabla \Gamma$ (see eq. (4)). This is non-zero when the particles are not uniform and hence particles exert a force on each other in order to reach an equilibrium position. Using the SPH approximation, the above equation is discretized as

$$a_{b,i} = \frac{d\mathbf{u}_i}{dt} = - \sum_j p_b \frac{V_i V_j}{m_i} \nabla W_{ij}, \quad (13)$$

where $V_i = \frac{m_i}{\rho_i}$ is the volume of the i^{th} particle, ρ_i is the density, W_{ij} is the kernel function chosen for the SPH discretization. The summation is over all the neighbors of i^{th} particle. Since all SPH kernels satisfy eq. (5), any suitable SPH kernel discussed in section 2 can be employed. In this paper, the quintic spline kernel is used given by,

$$W(q) = \begin{cases} \sigma [(3-q)^5 - 6(2-q)^5 + 15(1-q)^5] & \text{for } 0 \leq q \leq 1, \\ \sigma [(3-q)^5 - 6(2-q)^5] & \text{for } 1 < q \leq 2, \\ \sigma (3-q)^5 & \text{for } 2 < q \leq 3, \\ 0 & \text{for } q > 3, \end{cases} \quad (14)$$

where, $\sigma = 1/(120h), 7/(478\pi h^2), 1/(120\pi h^3)$ in one, two and three-dimensions respectively and $q = |\mathbf{r}|/h$. In this algorithm, the value of p_b is set to 1 independent of the resolution. In addition to this force, a repulsive force (RF)

similar to the gradient of the Lennard Jones potential (LJP) is used. The new repulsion force potential (ϕ_{RF}) is given by

$$\phi_{RF} = 12 k_r \left(\frac{c^2}{r^3} - \frac{c}{r^2} \right) \quad (15)$$

where k_r is a constant. We set $c = 2\alpha\Delta s/3$, where α is a scaling factor. The gradient of eq. (15) gives us the force due to ϕ_{RF} . The force is kept constant for $r < \Delta s/2$ in order to avoid very large repulsion forces. The SPH approximation of the acceleration due to eq. (15) can be written as

$$a_{RF,i} = -\nabla\phi_{RF,i} = \begin{cases} \sum_j 192 k_r \mathbf{e}_{ij} \left(\frac{3c^2}{\Delta s^4} - \frac{c}{\Delta s^3} \right) & r_{ij} \leq \Delta s/2 \\ \sum_j 12 k_r \mathbf{e}_{ij} \left(\frac{3c^2}{r_{ij}^4} - \frac{2c}{r_{ij}^3} \right) & \Delta s/2 < r_{ij} \leq \alpha\Delta s \\ 0 & r_{ij} > \alpha\Delta s \end{cases} \quad (16)$$

where $\mathbf{e}_{ij} = \mathbf{x}_{ij}/r_{ij}$. Note that the acceleration is continuous at $r_{ij} = \Delta s/2$. We find that using a value of $\alpha = 0.95$ works well for the algorithm.

It is clear from eq. (16) that this force is active only when particles come closer than the desired particle spacing. This prevents particle pairing, which may happen due to the use of some kernels like cubic spline for large time steps [32]. In fig. 5, the comparison between the force due to LJP and RF is shown. The LJP repulsion force increases rapidly compared to our suggested repulsion force. This allows us to use a larger time step during integration. Moreover, unlike the force due to LJP, the new force does not introduce inter-particle attraction.

As discussed in [12], for stability, a damping force is used to reduce the energy of the system. The acceleration due to damping for the i^{th} particle is given by

$$a_{d,i} = -\zeta \mathbf{u}_i \quad (17)$$

where ζ is the damping constant and \mathbf{u}_i is the velocity of the i^{th} . The value of the damping constant ζ is discussed in section 3.1.6. Thus, the equation governing the dynamics of the system is given by

$$\frac{du}{dt} = -\frac{\nabla p_b}{\rho} - \nabla\phi_{RF} - \zeta \mathbf{u} \quad (18)$$

The above equation can be converted into SPH form using eqs. (13), (16) and (17). It must be noted that the combination of background pressure force

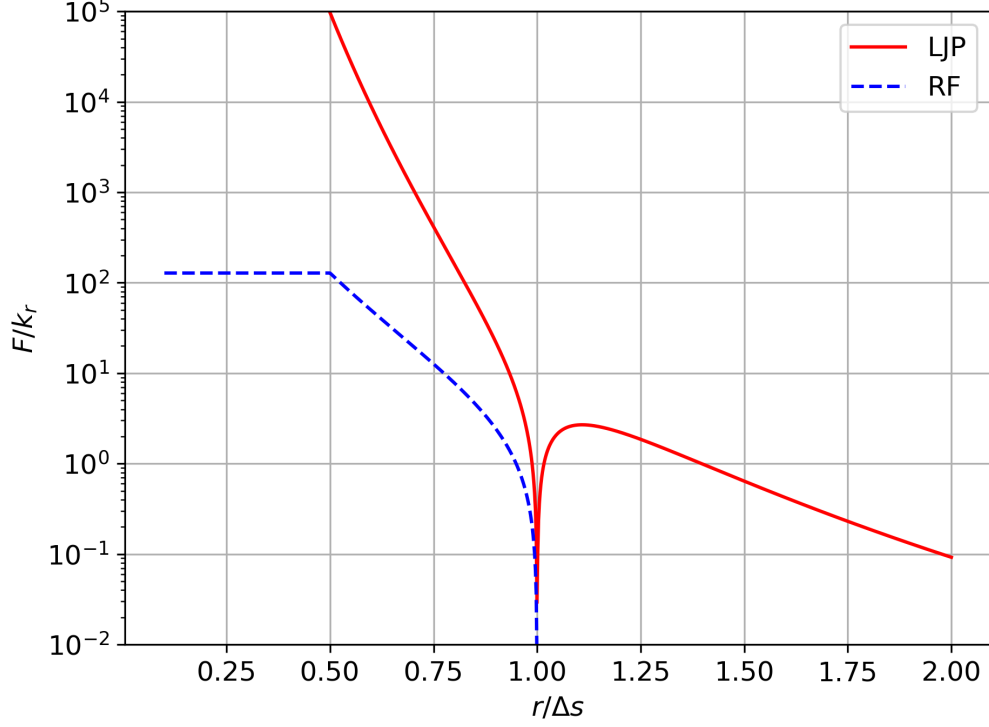


Figure 5: Force due to LJ potential and the gradient of eq. (15) as a function of distance, r and $\alpha = 1$.

and the repulsion force produces repulsion only when particles are disordered. This can also be accomplished by using the particle shifting techniques (PST) first proposed by [10].

On using eq. (18) the velocities and new positions are calculated using a semi-implicit Euler integration given by,

$$\begin{aligned} u_i(t + \Delta t) &= u_i(t) + \Delta t a_i(t) \\ r_i(t + \Delta t) &= r_i(t) + \Delta t u_i(t + \Delta t) \end{aligned} \quad (19)$$

In the case of boundary particles, the velocities are corrected to constrain them to move along the surface (discussed in section 3.1.4). It should be noted that the packing algorithm only ensures that particle distributions are regular and therefore using a higher order integrator would not promise better results.

The stability of the method in a two and three-dimensional domain for finite perturbation under the action of forces described above is studied. A domain of size 1 unit along each coordinate direction is considered. Particles are placed with a spacing of $\Delta s = 0.05$. Fixed particles are placed outside this unit box suitably. The value of p_b , ζ , k_r and Δt are set as discussed in section 3.1.6. A single particle close to the center is perturbed by $\Delta s/2$ in each direction. The particles are moved using eq. (18) and eq. (19) for 15000 iterations. The stability of the following initial distribution of particles is considered:

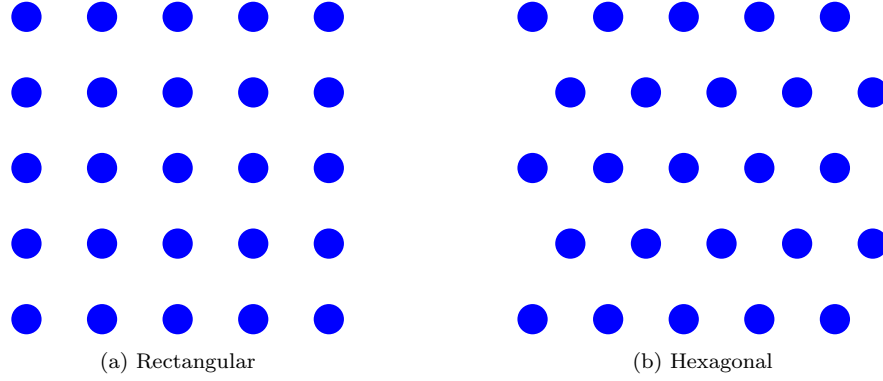


Figure 6: Different packing structures in 2D.

- hexagonal packing shown in fig. 6b with number density (ND) gradient.
- hexagonal packing shown in fig. 6b with $ND + \text{repulsion force } (RF)$.
- rectangular packing shown in fig. 6a with ND gradient.
- rectangular packing shown in fig. 6a with $ND + RF$.

The error in every iteration is evaluated using

$$L_{\infty}(\rho - \rho_o) = \max(\{(\rho_i - \rho_o), \forall i \in 1..N\}) \quad (20)$$

where N is the number of particles in the domain. In fig. 7a and fig. 7b the $L_{\infty}(\rho - \rho_o)$ is plotted with number of iterations for 2D and 3D domain respectively with $\rho_o = 1.0$. It is evident from the figure that in 2D, all the combinations perform well. In the case of the 3D domain, rectangular

lattices settle into an equilibrium configuration with a much larger density difference. Therefore the rectangular lattice in 3D is an unstable equilibrium. In contrast, the hexagonal packing in 3D is in a stable equilibrium.

This behavior in 3D can be understood from the total potential energy of the particles. It can be seen that eq. (3) for Γ_i is the potential energy of the i^{th} particle and hence $\sum_i \Gamma_i$ is the total potential energy of the system. The acceleration of a particle given in eq. (12) is the negative of the gradient of its potential energy. We have numerically found that a small perturbation of a particle at a given site reduces the total potential energy in the case of the rectangular lattice whereas, the same perturbation results in higher potential energy in the case of the hexagonal packing. This suggests that the hexagonal packing is stable in 3D unlike the rectangular lattice. A careful analysis on the stability is outside the scope of the present work. Due to the stability of hexagonal packing shown in fig. 6b, it is used in all our test cases.

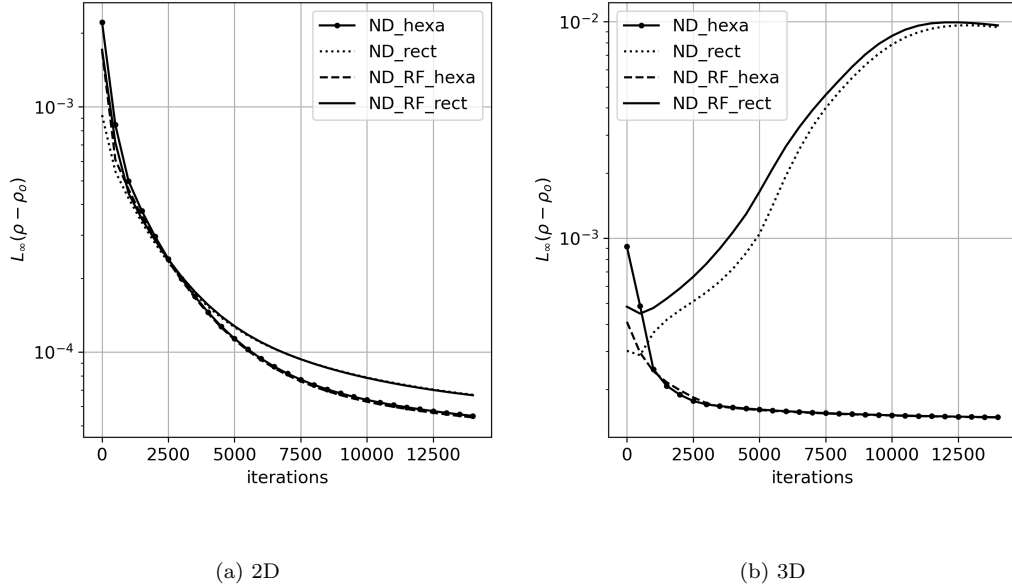


Figure 7: Density convergence with a particle at center perturbed by $\Delta s/4$.

3.1.3. Projecting free particles to the surface

Initially, the boundary particles are unlikely to conform to the boundary surface. At $t = 0$ no particles are assigned as boundary particles. Free particles are converted to boundary particles after every 50 iterations. This

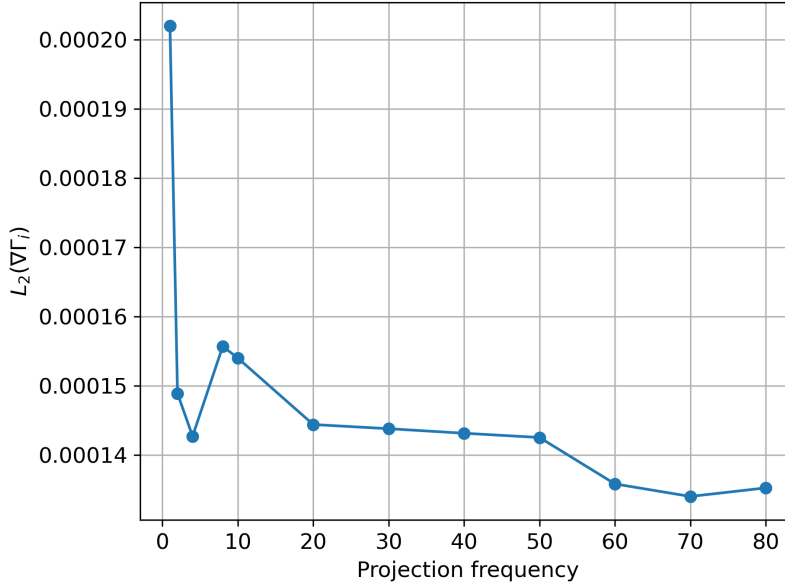


Figure 8: Error in $\nabla\Gamma_i$ for domain with unit radius cylinder with different projection frequency.

is called as the “projection frequency”. The projection frequency is a user-defined parameter. Increasing this does not guarantee better results however a very small value is not recommended. On running the proposed algorithm with spacing $\Delta s = 0.1$ around a unit radius 2D cylinder with varying projection frequency as shown in fig. 8, it was found that the after projection frequency 20, the number density gradient do not change by a large value. Thus, the value 50 is chosen heuristically.

If we consider a flat surface, an estimate for the number of particles that can fill the surface is, $N_s = A_s / \Delta s^{(d-1)}$ where A_s is the area of the surface and d is the dimension of the space in which the surface is embedded. In order to perform projection, two different criteria are employed depending upon whether the initial projection in fig. 2 is complete or not, as shown in algorithm 1.

In the algorithm, the function `FindParticlesNearBoundary` finds all the free particles that are less than a prescribed distance, `maxdist`, to a boundary node. The distance is computed as follows, given a free particle p , we find the boundary node b that is closest and compute the distance $\mathbf{r}_{pb} \cdot \mathbf{n}_b$, where $\mathbf{r}_{pb} = \mathbf{r}_p - \mathbf{r}_b$ and \mathbf{n}_b is the normal at b . It is to be noted that the algorithm to

Algorithm 1: Pseudo-code for free particle projection.

```
Input: proj_freq, ds= $\Delta s$ 
Result: List of free particles to be projected
iteration = 0;
empty_count = 0;
while not converged do
    ...;
    if iteration % proj_freq == 0 then
        if empty_count < 4 then
            p_list = FindParticlesNearBoundary(maxdist=0.5*ds);
            if len(p_list) > 0 then
                ConvertParticles();
                empty_count = 0;
            else
                empty_count++;
            end
        else
            p_list = FindParticlesNearBoundary(maxdist=0.65*ds);
            ConvertParticles();
        end
        ProjectToBoundary();
        ...;
    end
    iteration++;
end
```

find the nearest boundary node uses the existing neighbors generated when computing the accelerations discussed in section 3.1.2.

The `empty_count` variable stores the number of consecutive passes for which the `p_list` was empty. The free particles having a distance to the boundary node less than $0.5\Delta s$ are converted to boundary particles in `ConvertParticles` and projected to the boundary surface in `ProjectToBoundary`. However, if the `empty_count` exceeds 3, the distance threshold is increased to $0.65\Delta s$. This threshold is increased to handle the

corner cases where free particles are just outside $0.5\Delta s$ distance¹. This iterative conversion of free particles to boundary particles is necessary in order to capture the surface accurately.

3.1.4. Kinematics of boundary particles

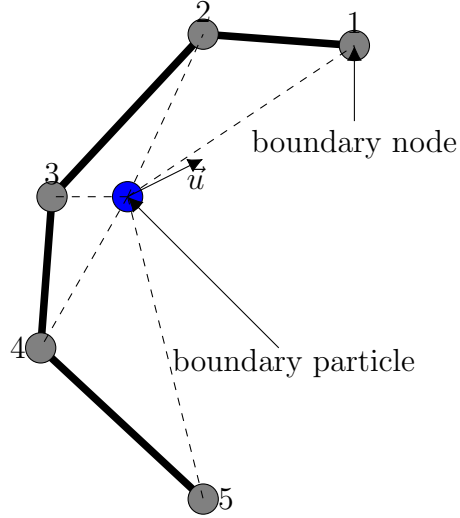


Figure 9: Motion of boundary particle along the geometry.

As discussed earlier, the movement of the boundary particles are constrained along the boundary surface. Figure 9 illustrates the motion of a boundary particle (in blue) along the geometry represented by nodes 1, 2, 3, 4, and 5. We note that even though the particle is a boundary particle, it is only projected onto the surface every `proj_freq` time steps as discussed in section 3.1.3 hence the boundary particle may not exactly lie on the boundary as it moves.

The motion of the boundary particle is performed as follows. The boundary node nearest to the boundary particles in the direction of the particle's velocity is identified. Consider a boundary particle p , and a boundary node j , near p having position \mathbf{x}_p and \mathbf{x}_j respectively. The index of the nearest

¹This value was found based on numerical experiments. Too small a value like $0.55\Delta s$ produces poor results in coarse resolutions and too large a value ($0.75\Delta s$) produced poor distributions with finer resolutions.

node, J is determined by

$$J = \arg \min_j \{r_{pj} \mid j \in \mathcal{N}_p \text{ and } \mathbf{x}_{pj} \cdot \mathbf{u}_p < 0\} \quad (21)$$

where, $\mathbf{x}_{pj} = \mathbf{x}_p - \mathbf{x}_j$, $r_{pj} = |\mathbf{x}_{pj}|$, \mathbf{u}_p is the velocity of the boundary particle and \mathcal{N}_p is the set of neighboring nodes of p . In fig. 9, the node 2 satisfies the conditions in eq. (21), and so $J = 2$. Using the nearest node index J , and the boundary particle p , the direction of motion $\hat{\mathbf{x}}_r = -\hat{\mathbf{x}}_{pJ}$ (where $\hat{\mathbf{x}} = \mathbf{x}/|\mathbf{x}|$). Thus, the boundary particle position is updated using the following equation

$$\mathbf{x}_p^{m+1} = \mathbf{x}_p^m + (\mathbf{u}_p^{m+1} \cdot \hat{\mathbf{x}}_r^m) \hat{\mathbf{x}}_r^m \Delta t, \quad (22)$$

where m is the time step.

3.1.5. Convergence criteria

For a perfectly packed distribution of particles, each particle should satisfy the second condition in eq. (6) i.e. $\nabla \rho_i = 0$. However, this would take a lot of computational time. In case of geometries having irrational volumes like the unit circle ($V=\pi$), one could never achieve a perfect convergence, given a fixed resolution. Thus, similar to [24], the following criteria for convergence is used

$$\frac{\max(u_i) \Delta t}{h} < \epsilon \quad (23)$$

where, $\epsilon = 10^{-4}$ is the tolerance for all our test cases, u_i is the velocity magnitude of i^{th} particle, and the maximum is taken over all the particles.

3.1.6. Determining the constants and time-step

It is important to choose the parameters ζ and k_r appropriately. It can be seen that the eq. (13) scales as $O(p_b \Delta s^{-1})$ and eq. (16) scales as $O(k_r \Delta s^{-2})$. By requiring that these forces be of the same order, it can be seen

$$\frac{k_r}{p_b} = C \Delta s \quad (24)$$

where C is an arbitrary constant. To find a suitable value, a 2D lattice of points is considered. A single particle is perturbed by $\Delta s/4$ in each direction. A similar procedure is applied on a 3D lattice. A value of C in the range $0.004 - 0.006$ was found in order to ensure that the two forces are of the same order.

In order to ensure stability, the damping constant has a form similar to the one suggested by Colagrossi et al. [12] given by $\zeta = C_\zeta/\Delta s$, where C_ζ is set in the range $0.2 - 0.5$ resulting in an underdamped system.

The time step, Δt is set as in Adami et al. [11] given by,

$$\begin{aligned}\Delta t_{p_b} &= 0.1 \frac{h}{p_b} \\ \Delta t_\zeta &= \sqrt{0.1 \frac{h}{\zeta u_i}} \\ \Delta t &= \min(\Delta t_{p_b}, \Delta t_\zeta)\end{aligned}\tag{25}$$

where u_i is the velocity magnitude of the i^{th} particle. We note that we have used a $p_b = 1$ for all our simulations.

3.1.7. Separating interior and exterior particles

At the end of the simulation, both interior (particles inside the boundary surface) and exterior particles (particles outside the boundary surface) are uniformly distributed. The interior particles along with the boundary particles are extracted and used as solid particles, while the rest of the particles are used as fluid particles. In order to detect interior and exterior particles, this simple SPH based procedure is adopted:

- Step 1: Find the nearest boundary node j to free particle i . Let the normal at the point j be $\hat{\mathbf{n}}_j$.
- Step 2: If $\mathbf{x}_{ij} \cdot \hat{\mathbf{n}}_j > 0$ then the particle i is outside, otherwise it is inside.
- Step 3: Step 1 – 2 are performed for all particles near the boundary surface. For particles that are not near the boundary surface, the neighbors of the given particle are checked. If a neighbor is an exterior particle, then it too is an exterior particle, otherwise, it is an interior particle. This works because all particles near a boundary are already marked.

This process provides a simple method of identification of the interior and exterior particles. It must be noted this is done after the packing procedure is completed. This procedure takes much less computational time compared to the packing procedure.

3.1.8. Implementation

The algorithm is implemented using the open-source package PySPH [25]. The pseudo-code of the proposed hybrid method is shown in algorithm 2. The

nearest neighbor particle search (NNPS) algorithm implemented in PySPH [25] is not a part of the current algorithm.

The algorithm first reads the input using `ReadInput` and initialize the particles in `CreateParticles` as discussed in section 3.1.1. The constants and time step are set in `SetConstantAndTimeStep`. The first iteration starts with `UpdateNeighbors` where the neighbor list for every particle is created. This is followed by acceleration computation in `ComputeAccelerations` and integration in `IntegrateParticles` as discussed in section 3.1.2 and section 3.1.4. Nearest free particles are converted and projected to the surface in `ProjectParticles` as discussed in section 3.1.3. This procedure updates the `empty_count` variable. The iterations continues until convergence condition is true in `CheckConvergence` as discussed in section 3.1.5. Finally, the particles are separated into internal and external particles in `SeparateParticles` as discussed in section 3.1.7.

Algorithm 2: Hybrid particle packing algorithm.

```

Result: Coordinates of solids and fluids
ReadInput();
CreateParticles();
SetConstantAndTimeStep();
p_freq = 50;
iteration = 0;
empty_count = 0;
converged = False;
while not converged do
    UpdateNeighbors();
    ComputeAccelerations();
    IntegrateParticles();
    if iteration % p_freq == 0 then
        empty_count = ProjectParticles(empty_count);
        if empty_count > 4 then
            converged = CheckConvergence();
        end
    end
    iteration++;
end
SeparateParticles();

```

3.1.9. Obtaining faster convergence

The algorithm discussed above is the basic form, which adds particles slowly to the boundary. In case when the boundary surface is smooth and does not have sharp changes (as discussed in section 3.1.1), the following approaches can be taken to speed up the packing process:

- Using surface point prediction: When the boundary is smooth one may project $0.9N_s$ immediately at the start. This perturbs the distribution of the particles significantly. If required more particles are projected to the boundary while settling the system to an equilibrium.
- Filter layers near the boundary surface: Conforming particles to the boundary surface requires that only some of the particles be moved. Thus, one could filter the free particles near the boundary surface and freeze the other particles.
- Reduce projection frequency: One can reduce it slowly once the initial projection is complete.
- Reduce the convergence tolerance: One can potentially reduce the tolerance to increase the performance of the algorithm, although this would reduce the quality of the distribution of particles.

Doing these can potentially reduce the computations by up to a factor of two. However, we have not performed any of these in the results presented here.

3.2. Standard Packing

In this method, the interior of a 2D object is constructed by using the method proposed by Marrone et al. [20]. The object boundary is represented by a piecewise linear curve (PLC) with normals to the boundary pointing out of the solid. The first layer of the interior is generated by moving the PLC points into the body along the normal by $\Delta s/2$ where Δs is the particle spacing. The new PLC is discretized into particles such that each particle is approximately Δs distance apart along the PLC. The newly added PLC is moved further into the body along the normal by Δs and discretized again. This procedure is repeated until the desired number of layers of solid particles are generated. It must be noted that this works only for 2D objects.

Once the dummy layers representing the solid body is created, fluid particles are placed around the solid particles. The method proposed by Colagrossi

et al. [12] is used to pack particles around the fixed solid particles. In order to initialize the particle position, a grid of evenly distributed particles is considered and only the particles outside (defined by the direction of normal) the boundary surface represented by the PLC are retained. The particles are packed using the number density gradient. It must be noted that since only the number density gradient is used as a repulsion force amongst the particles, they are prone to clumping [33, 34]. The particles are subjected to a damping force to dissipate the energy of the system. Hence the force on any particle is governed by

$$\frac{d\mathbf{u}}{dt} = -\frac{\nabla p_b}{\rho} - \zeta \mathbf{u}, \quad (26)$$

The value of p_b and ζ is set directly as described in section 3.1.6. The same SPH discretization is used as done in equation eq. (13) and eq. (17). The convergence criteria remain the same as discussed in section 3.1.5.

Algorithm 3: Standard particle packing algorithm.

Result: Coordinates of solids and fluids

```

ReadInput();
CreateParticles();
SetConstantAndTimeStep();
converged = False;
iteration = 0;
while not converged do
    UpdateNeighbors();
    ComputeAccelerations();
    IntegrateParticles();
    converged = CheckConvergence();
    iteration++;
end

```

In algorithm 3 the standard packing is described in detail. The `ReadInput` functions reads the points describing the geometry. All the particles are initialized and the dummy particles are created using method proposed by Marone et al. [20] in `CreateParticles`. The `SetConstantAndTimeStep` function sets the constants and time step as discussed in section 3.1.6. The iteration starts with creation of neighbor lists for every particle in `UpdateNeighbors`.

Then, accelerations are computed in `ComputeAccelerations` using eq. (26) and integrated in `IntegrateParticles` using eq. (19). The iteration continues until the criteria described in section 3.1.5 is satisfied in `CheckConvergence`.

3.3. Coupled packing

Jiang et al. [24] proposed a packing algorithm for solid objects both in 2D and 3D in order to sample blue noise. The steps involved are described in algorithm 4. A repulsion force which is similar to the one used in [12] is used along with damping. However a symmetric form of SPH discretization is used given by

$$a_{b,i} = -m_i p_b \sum_j m_j \left(\frac{1}{\rho_i^2} + \frac{1}{\rho_j^2} \right) \nabla_i W_{ij}, \quad (27)$$

where W_{ij} is the cubic spline kernel function. This is computed in `ComputeAccelerations` along with an additional force discussed later. In the present implementation, a constant background pressure, p_b is used. In the original method $p_b = \eta(\rho - \rho_o)$ where η is a constant. On computing the acceleration, all the particles are integrated in `IntegrateParticles`.

Since the particles near the surface lack supporting particles, a large force acts upon them. In order to keep the particles inside a confined region, the particles nearer than $0.05\Delta s$ are converted to boundary particles. These are integrated similarly as in the case of the hybrid method described in section 3.1.2. The boundary particles are projected back to the surface in every iteration in `ProjectParticles` as done in the original method.

Algorithm 4: Packing algorithm by Jiang et al. [24].

```

Input: particles, max_iter
Result: Packed particles
iteration = 0;
while not converged and iteration < max_iter do
    UpdateNeighbors(particles);
    ComputeAccelerations();
    IntegrateParticles();
    ProjectParticles();
    iteration++;
end
```

If one were to only use eq. (27), it would result in more number of particles pushed towards the boundary. In order to counteract the force on the particles near the boundary, Jiang et al. [24] used a cohesion force proposed by Akinici et al. [35]. The acceleration due to this force in SPH form is given by

$$a_{c,i} = -m_i \gamma \sum_j m_j k_{ij} C_{ij} \hat{\mathbf{n}}_{ij} \quad (28)$$

where $k_{ij} = 2\rho_o/(\rho_i + \rho_j)$, $\hat{\mathbf{n}}_{ij} = \mathbf{x}_{ij}/r_{ij}$ and C_{ij} is the spline kernel in [35] given by

$$C(q) = \frac{32}{\pi h^d} \begin{cases} (1-q)^3 q^3 & 0.5 < q < 1 \\ 2(1-q)^3 q^3 - \frac{1}{64} & 0 < q < 0.5 \\ 0 & \text{otherwise} \end{cases} \quad (29)$$

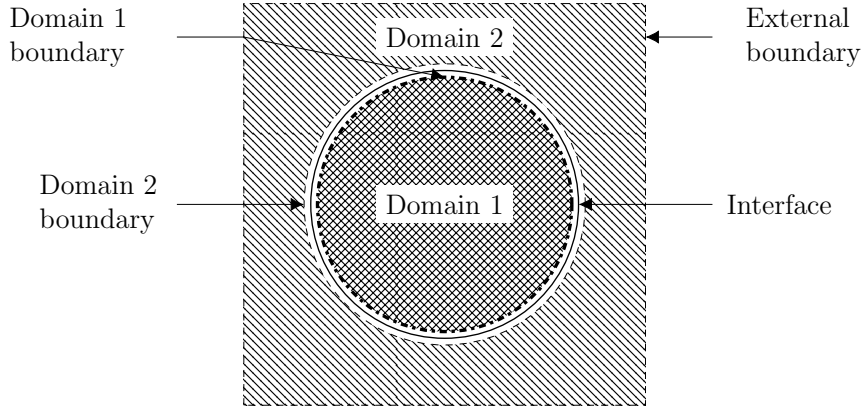


Figure 10: Schematic for the coupled packing algorithm. The external region is marked as domain 2 and the internal region is marked as domain 1.

Jiang et al. [24] have not specified a way to choose the value of the constants in eq. (27) and eq. (28). The values of $\gamma = 20$, $p_b = 10$ and $h = \Delta s$ are heuristically chosen for all the simulations.

It must be noted that there is no exterior defined in [24]. In this work, the exterior is also packed in the same manner as the interior by moving the boundary surface by $\Delta s/2$ and $-\Delta s/2$ for exterior and interior respectively. In fig. 10, the interior domain (domain 1) is enclosed within a thick dashed line and the exterior is within a thin dashed line (domain 2). Each domain is represented with a different pattern. Domain 2 having an external boundary has frozen particles outside it. The solid line represents the boundary surface.

Algorithm 5: Coupled particle packing algorithm.

Result: Coordinates of solids and fluids

```
ReadInput();
DivideDomain();
CreateParticles();
SetConstantAndTimeStep();
Algorithm4(domain1, 5000);
Algorithm4(domain2, 5000);
iteration = 0;
converged = False;
while not converged do
    UpdateNeighbors(domain1 + domain2);
    ComputeAccelerations();
    IntegrateParticles();
    converged = CheckConvergence();
    iteration++;
end
SeparateParticles();
```

The particles are packed in two different passes as described in algorithm 5. First, the geometry data is read in `ReadInput` followed by particle initialization in `CreateParticles`. The free particles are divided into domain 1 and domain 2 depending upon their location in `DivideDomain`. For particles that are lying in between the two dashed boundaries of domain 1 and 2, the following is done. If a particle is in the exterior region (outside the boundary surface) it is moved along the normal by a distance Δs into domain 2. Similarly, particles between the boundary surface and the domain 1 boundary are moved into domain 1.

In the first pass, domains 1 and 2 are solved separately using the algorithm 4. In this case, each domain is unaware of the other. The boundary particle projection is performed onto the dashed lines of the respective boundaries. The particles in both the domains are moved for a predetermined number of iterations at which point the particles reach equilibrium². This ensures that

²The predetermined iterations is chosen as 5000 currently based on the test cases considered.

all particles are sorted as either interior or exterior and have an interface which they cannot cross i.e. the dashed lines.

In the second pass, when the projection is complete, the particles on the interior surface i.e. the thick dashed line are constrained to move along it. All other particles are allowed to freely move using eq. (27) in `ComputeAccelerations` and `IntegrateParticles`. The iteration continues until the convergence criteria in `CheckConvergence` as discussed in section 3.1.5 is satisfied. The presence of exterior particles eliminates the need for the cohesion force and is not added once domains 1 and 2 start interacting. Using this approach, a uniform distribution is obtained both inside and outside the surface. It is noted that the original implementation was used to sample blue noise and does not require external particles.

The proposed algorithms are implemented in the open-source SPH framework, PySPH [25]. The present implementation is open source and freely available with this manuscript at https://gitlab.com/pypr/sph_geom. All the results shown in the next section are fully reproducible using a simple automation framework [36].

4. Results and discussion

In this section, all the algorithms discussed above are compared. The algorithms are first compared for a circular cylinder and a Z shaped wall in two dimensions. The standard method is limited to two-dimensional domains. Hence, in three-dimensions, only the coupled and the hybrid method are compared for an ellipsoid. We also show the particle distribution for a symmetric airfoil and an arbitrarily shaped geometry using the hybrid method at different resolutions. In the end, we demonstrate the hybrid algorithm for a complex-shaped Stanford bunny.

4.1. Circular cylinder

The flow of an incompressible fluid past a cylinder is a well-known benchmark problem. In order to obtain a good comparative study, one desires to remove the effect of the surface irregularities due to the underlying method of geometry creation. In this test case, the circular cylinder constructed using all the approaches discussed in section 3 are compared. A cylinder of diameter $D = 2m$ is considered. In fig. 11, the geometry with particle spacing $\Delta s = 0.1$ made using different methods is shown. It is clear that the hybrid method produces a uniform particle distribution. In the case of the

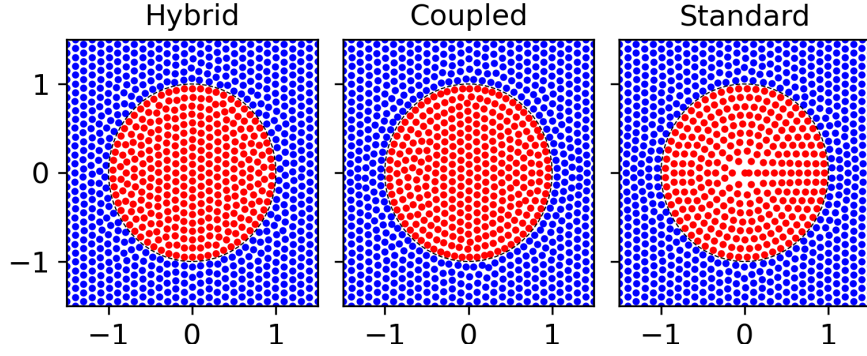


Figure 11: Solid (Red) and fluid (Blue) particles for a circular cylinder for $\Delta s = 0.1$.

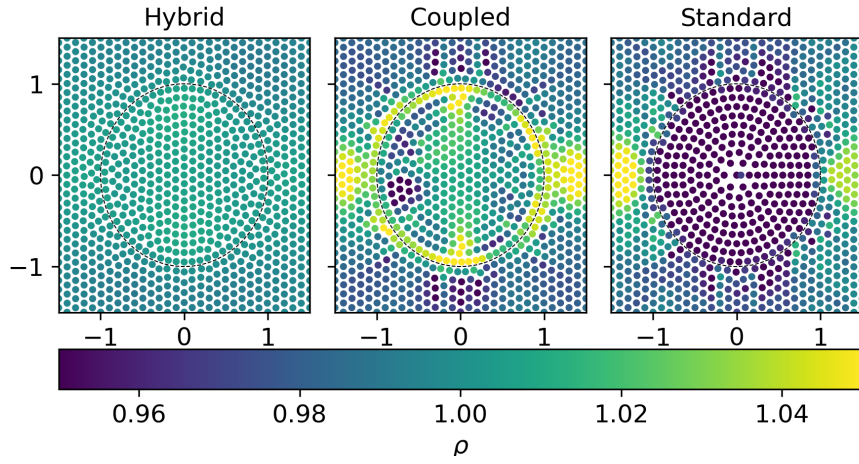


Figure 12: Density distribution of the packed particles for the circular cylinder geometry for $\Delta s = 0.1$.

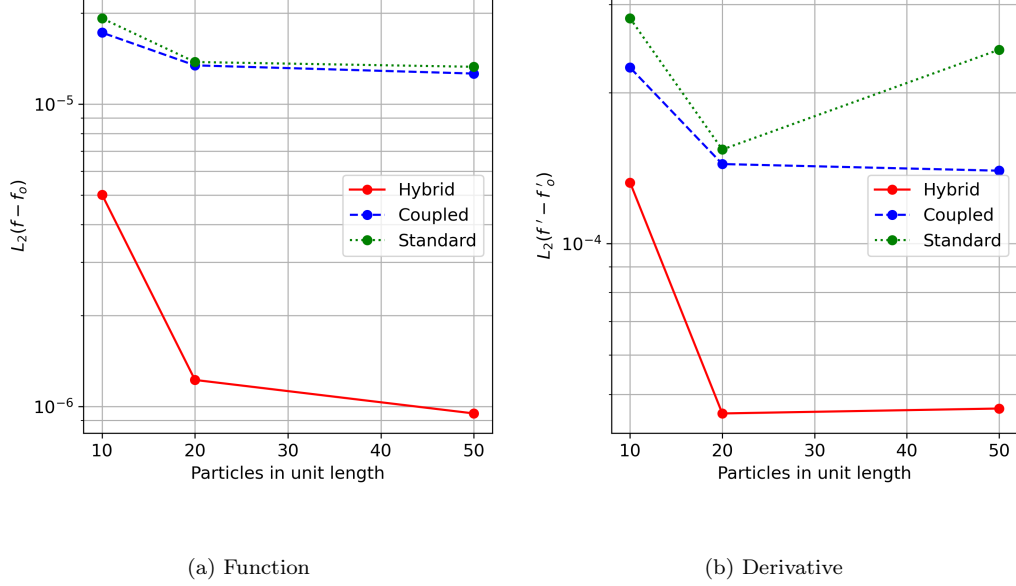


Figure 13: L_2 error for SPH approximation of function and its derivative for the circular cylinder geometry.

coupled method, a large number of particles near the wall surface is seen. The standard method seems to have uniform particles owing to its construction. In order to investigate this further, the density distribution is plotted as shown in fig. 12. The density distribution is obtained using the well-known summation density. Clearly, the coupled method shows high density near the surface and the standard method shows a low density on the solid since Δs particle distance is assumed over a curved surface. The total density variation is 8%, 16%, and 2% for the standard, coupled and hybrid methods respectively. Thus, it is clear that the proposed hybrid method shows excellent distribution with a maximum variation of 2%.

The improvement is studied quantitatively by interpolating a C_∞ function over the packed particles given by

$$f(x, y, z) = \sin(x^2 + y^2 + z^2). \quad (30)$$

The function and its derivative is approximated using

$$\langle f(\mathbf{x}) \rangle = \sum_j f(\mathbf{x}_j) W_{ij} \frac{m_j}{\rho_j} \quad (31)$$

and

$$\langle f_x(\mathbf{x}) \rangle = \sum_j f(\mathbf{x}_j) W_{ij,x} \frac{m_j}{\rho_j} \quad (32)$$

respectively. The L_2 error in the approximation is evaluated using

$$L_2(f - f_o) = \frac{\sqrt{\sum_j (f(\mathbf{x}) - f_o(\mathbf{x}))^2}}{N} \quad (33)$$

where, f_o is the SPH function approximation on a regular mesh of points. The value of the function is set as per the position of each particle as $f(\mathbf{x}_i)$. This is then interpolated onto a regular mesh using eqs. (31) and (32). The same is done for the regular points themselves to obtain the reference f_o value at each point. The value of h is varied in order to get convergence. A value of $h/\Delta s = 1.0$ is taken for $\Delta s = 0.1$ and linearly varied to $h/\Delta s = 1.5$ for $\Delta s = 0.02$. The quintic spline kernel is used for the interpolation. When comparing the derivatives, only the x derivative is considered. In fig. 13a and fig. 13b, $L_2(f - f_o)$ and $L_2(f' - f'_o)$ are shown. In these plots the errors near the center of the cylinder are not evaluated as they do not affect the flow and the standard method performs poorly in this region. This change allows for a fair comparison. Hence, the L_2 norm is evaluated only over the points where $r > 0.45 D$. It is clear that the hybrid method shows a significant order of magnitude improvement compared to both coupled and standard methods. The coupled method is slightly better than the standard method. The standard method shows large error due to the way in which the surface is represented.

4.2. Zig-Zag Wall

The zig-zag wall is one of the test cases proposed by Marrone et al. [20] used to demonstrate the δ -SPH method. They employ the standard packing algorithm in order to generate a solid body and pack the fluid particles around. In this test case, particles are packed using all the algorithms and compared. The zig-zag wall is an excellent test case for packing since it has both concave and convex sharp edges. In order to generate a solid using the standard method, the corner nodes are moved along the angle bisector and uniform points are generated using these points as endpoints. In the other algorithms, these sharp points are referred as corner nodes and the method discussed in section 3.1.2 is employed to automatically restrict the motion of these points.

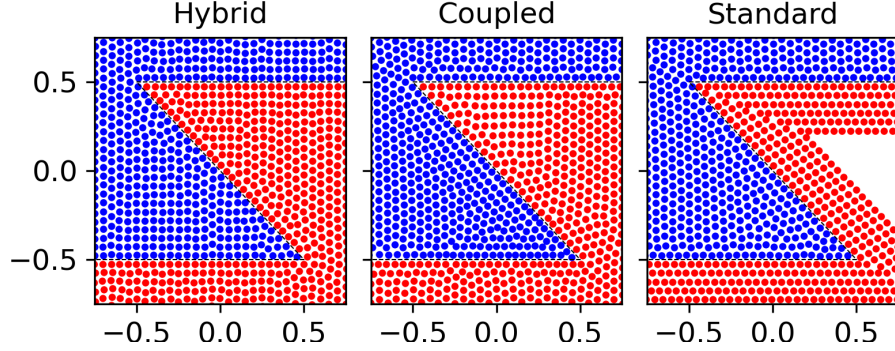


Figure 14: Solids (Red) and fluids (Blue) for the zig-zag wall for $\Delta s = 0.05$.

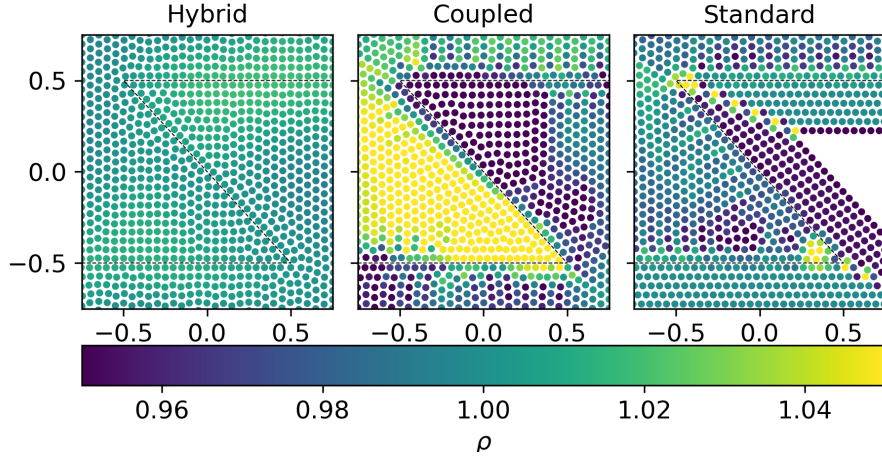


Figure 15: Density distribution for the zig-zag wall for $\Delta s = 0.05$.

In fig. 14, the solid and fluid particles packed with $\Delta s = 0.05$ using different algorithms are shown. It is difficult to conclude which of these is better. However on looking at the density distribution computed using the summation density as shown in fig. 15 one can clearly see that the proposed method has much less deviation from the desired density. In the case of the coupled method, higher density is observed at the concave corner. This occurs since the particles from both sides push towards the interface at the first pass of the coupled algorithm as discussed in section 3.3. The standard method shows an uneven variation of density near the sharp edges which is not desirable. The total density variation is 10%, 30% and 3% for standard, coupled and hybrid methods respectively. It clearly shows that the hybrid

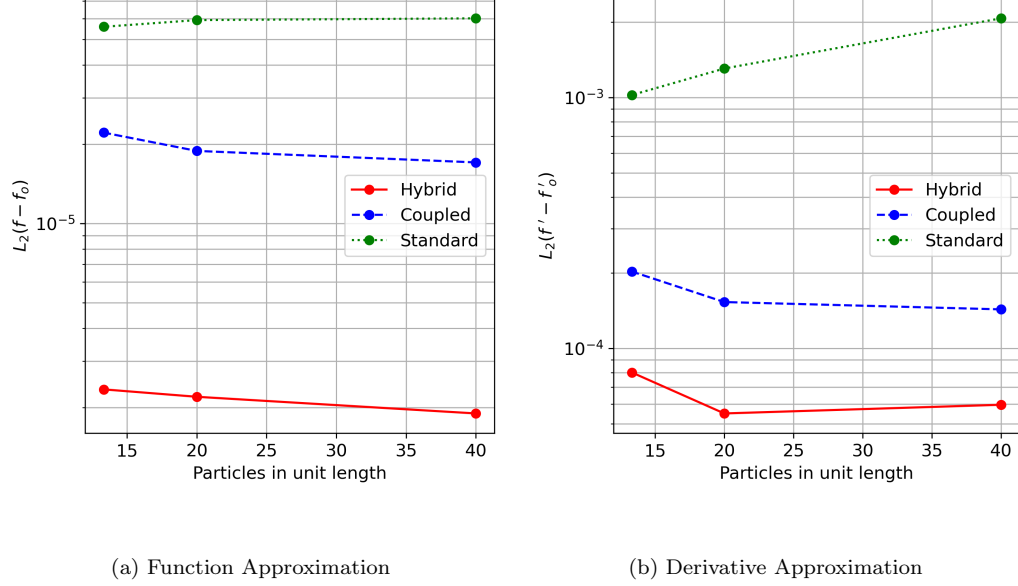


Figure 16: L_2 error for SPH approximation of function and its derivative for the zig-zag wall.

method shows very small density variations compared to other methods.

A similar analysis over the zig-zag wall is performed as done in the case of the cylinder. In order to remove the effect of the interior of the solid in the standard case, the errors are computed only up to a distance of Δs inside the wall. In fig. 16a and fig. 16b, L_2 norm for the error in function and its derivative SPH approximation is plotted respectively. Clearly, the proposed method performs very well as compared with the other methods.

4.3. Packing at different resolutions

In this example, the hybrid algorithm is applied on an arbitrary shaped body. The packing at different particle spacings are shown in fig. 17. The particle spacings chosen are 0.05, 0.075, and 0.1. The particles are placed at $\Delta x/2$ distance away from the boundary. Clearly, the density distribution is close to the desired value of 1.0. The particles conform to the body surface and has a total variation of density of 2.5%, 2% and 3% for particle spacing 0.1 and 0.075 and 0.05 respectively. This shows that the proposed algorithm is applicable to complex two-dimensional geometries.

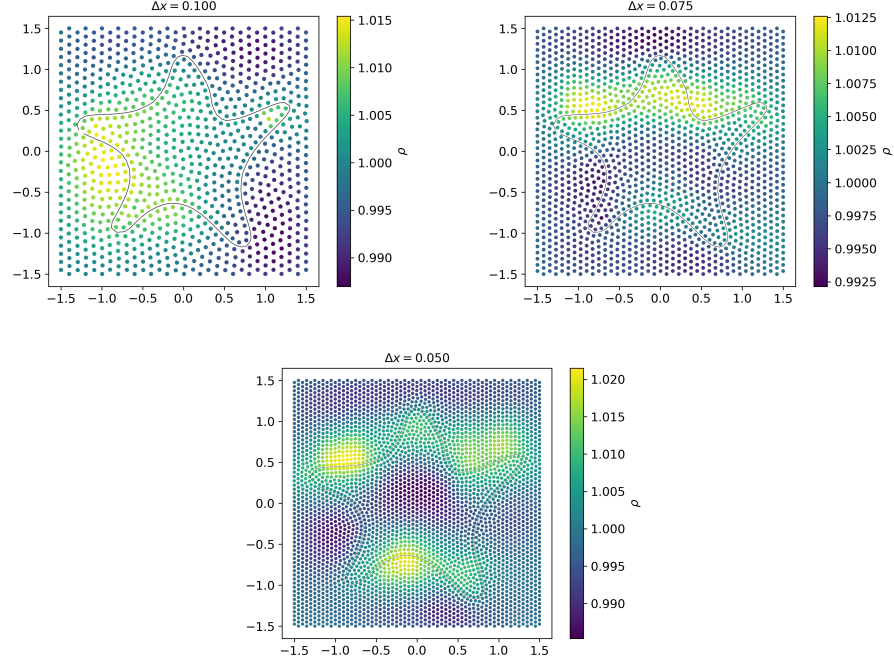


Figure 17: Density distribution at different resolutions for an arbitrary shaped object.

4.4. Effect of convergence tolerance on the quality

In this test case, we show that the proposed algorithm can achieve a high-quality particle distribution for a given tolerance. A symmetric airfoil, NACA0015 is considered. The end-point at the trailing edge is chosen as a corner node. Particle packing is performed using the proposed hybrid method for the spacing $\Delta s = 0.02$.

In table 1, the number of iterations required for convergence and the L_∞ error in the density for different values of the tolerance required for convergence are tabulated. It is evident from the table that the L_∞ error decreases with the decrease in the tolerance however, the number of iteration required increases significantly. In the fig. 18, we show the high-quality particle distribution achieved using a lower value of tolerance, $\epsilon = 2.5 \times 10^{-5}$ in the convergence criteria. It shows that the proposed method can achieve a high-quality particle distribution provided a sufficiently low tolerance is used.

Tolerance	Iterations	$L_\infty(\rho_i)$
2.5e-05	19641	0.011
5.0e-05	6291	0.019
1.0e-04	1191	0.028

Table 1: The table shows the effect of the change in tolerance for convergence on the number of iterations and the L_∞ error in the density.

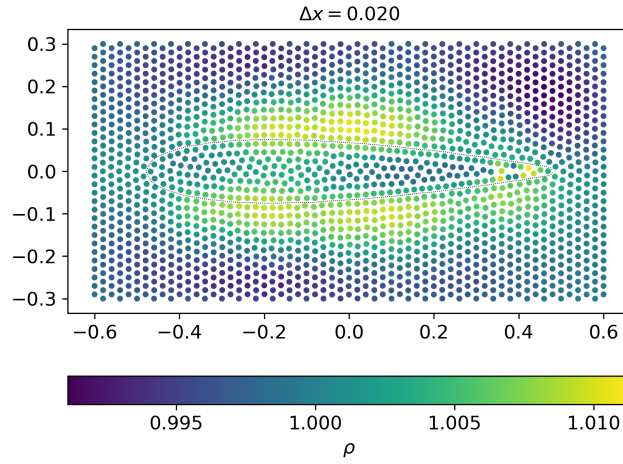


Figure 18: The density distribution for a symmetric airfoil with particle spacing, $\Delta s = 0.02$ and convergence tolerance, $\epsilon = 2.5e^{-5}$.

4.5. Particle Packing in 3D

One of the advantages of the proposed algorithm is that it can be easily extended to a three-dimensional object unlike the standard method. In order to compare the packing in 3D, particles are packed for a simple ellipsoid. The ellipsoid has semi-major axis dimensions, $a = 1.0$, $b = 0.5$ and $c = 0.75$ along x , y and z axis respectively. In fig. 19a and fig. 19b, the packed particles over the surface of the sphere for hybrid and coupled method are shown respectively. The color of the particles show the density distribution. In order to show that the particles conform to the surface, the surface is pulled along the normal by $\Delta s/2$. It is clear that the hybrid method attains a good distribution of particles resulting in a density distribution very close to $\rho_o = 1.0$. The particle distribution using the coupled method has density near the

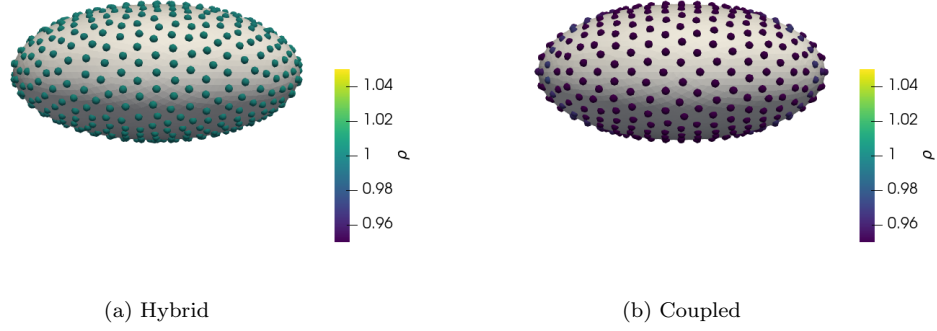


Figure 19: Density distribution on the surface of the ellipsoid for $\Delta s = 0.1$.

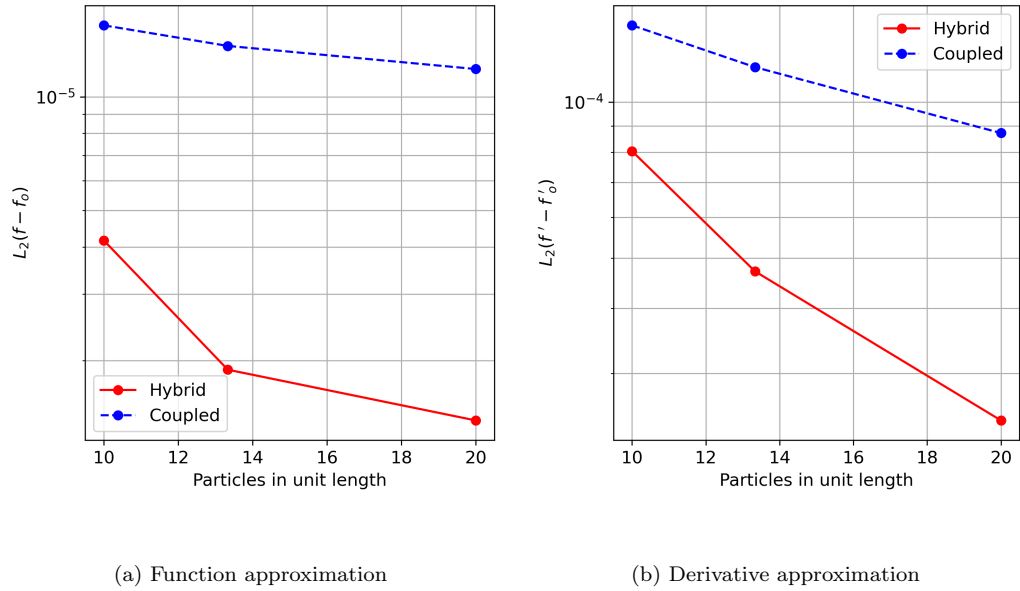


Figure 20: L_2 error for SPH approximation of function and its derivative for the ellipsoid.

lower range of the scale. This is due to the fact that unlike the hybrid method, the coupled method does not project the required number of particles on the surface. In order to perform a quantitative analysis, again the comparison of the function and derivative approximation used earlier is adopted. In fig. 20a and fig. 20b, L_2 error in SPH approximation of function and its derivative is plotted respectively. As can be seen, the proposed method produces much

lower errors at lower resolutions.

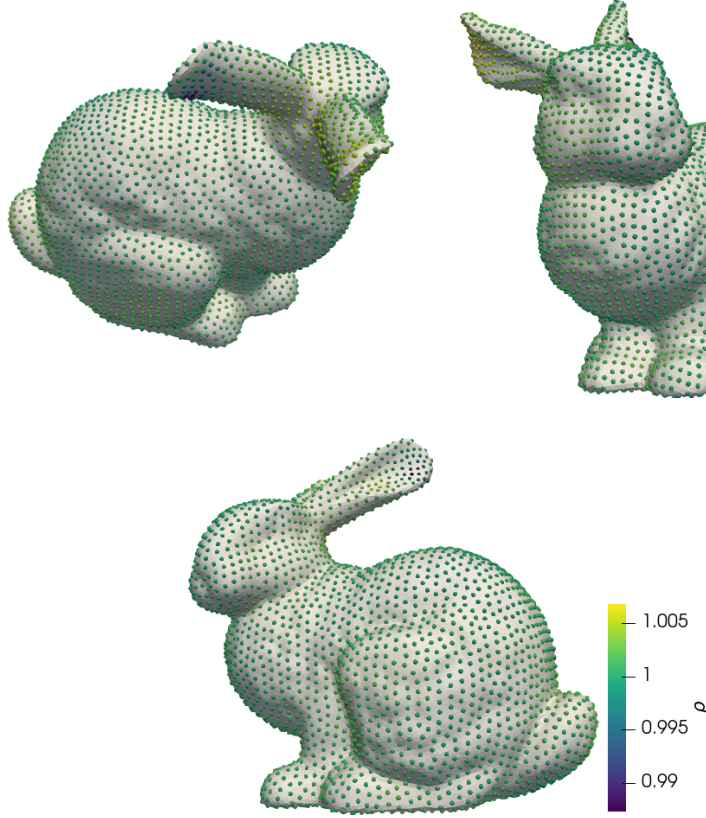


Figure 21: Different views showing particles (colored with density values) over the Stanford bunny.

In order to show the capability of the algorithm, the proposed algorithm is also applied to the Stanford bunny geometry, as done by Jiang et al. [24]. The geometry surface required must have outward normals, and the mesh is corrected using a mesh manipulation tool. A particle spacing of 0.02 is chosen. In this case, the intention is to show how well the geometry is captured, so the surface is not shifted inside. In fig. 19b, the particle distribution over the surface of the bunny is shown. The results show the applicability of the proposed algorithm to arbitrary shaped 3D objects. After pre-processing the 3D object can be placed anywhere in the domain, with the surrounding particles.

5. Conclusions

This paper proposes an improved particle packing algorithm for the simulation of flows involving complex geometries in two and three dimensions. Three different methods for packing particles around an arbitrary shaped object are implemented and compared. The standard method which is proposed by Colagrossi et al. [12] along with the solid object construction proposed by Marrone et al. [20]. A modified version of that proposed by Jiang et al. [24] which handles both the interior and exterior of the body. A new method that combines the best features of these methods is proposed. The proposed method provides an excellent density distribution as a result of evenly distributed particles. The method is applicable to both 2D and 3D domains. Unlike the coupled method, no estimation of particles inside and outside is required. Several benchmark cases are shown which highlight the accuracy of the proposed algorithm in two and three dimensions. An open-source implementation of the manuscript is provided and the manuscript is fully reproducible.

The SPH method is being applied to a wide variety of problem domains involving complex geometries. While mesh-free particle methods do not require a mesh, one must still capture the boundaries accurately. However, there are not many tools to create good quality initial particle distributions. This is necessary for accurate simulation of incompressible fluid flows with the SPH. The proposed method is largely automatic and offers researchers the ability to easily discretize complex geometries using particles in two and three dimensions. Since the proposed algorithm is based on the SPH, it should be easy to incorporate into an SPH solver. The code is also open source and hence researchers could also choose to use our implementation.

In the future, we would like to make it easier to use and integrate with the main PySPH package. We have only demonstrated our implementation on the CPU. However, PySPH supports execution on a GPU and we propose to make the necessary modifications for efficient execution on the GPU. The method currently works best for a fixed resolution. In the future it would be useful to explore this in the context of adaptive resolution.

References

References

1. Gingold, R.A., Monaghan, J.J.. Smoothed particle hydrodynamics: Theory and application to non-spherical stars. *Monthly Notices of the Royal Astronomical Society* 1977;181:375–389. doi:10.1093/mnras/181.3.375.
2. Lucy, L.B.. A numerical approach to testing the fission hypothesis. *The Astronomical Journal* 1977;82(12):1013–1024. doi:10.1086/112164.
3. Liu, M.B., Liu, G.R.. Smoothed Particle Hydrodynamics (SPH): an Overview and Recent Developments. *Archives of Computational Methods in Engineering* 2010;17(1):25–76. URL: <http://link.springer.com/10.1007/s11831-010-9040-7>. doi:10.1007/s11831-010-9040-7.
4. Violeau, D.. Fluid mechanics and the SPH method: theory and applications. 1st ed ed.; Oxford University Press; 2012. ISBN 978-0-19-965552-6. OCLC: ocn776772541.
5. Ye, T., Pan, D., Huang, C., Liu, M.. Smoothed particle hydrodynamics (SPH) for complex fluid flows: Recent developments in methodology and applications. *Physics of Fluids* 2019;31(1):011301.
6. Monaghan, J.J.. Smoothed Particle Hydrodynamics. *Reports on Progress in Physics* 2005;68:1703–1759.
7. Basa, M., Quinlan, N.J., Lastiwka, M.. Robustness and accuracy of SPH formulations for viscous flow. *International Journal for Numerical Methods in Fluids* 2009;60:1127–1148.
8. Kiara, A., Hendrickson, K., Yue, D.K.. SPH for incompressible free-surface flows. Part I: Error analysis of the basic assumptions. *Computers & Fluids* 2013;86:611–624. URL: <https://linkinghub.elsevier.com/retrieve/pii/S0045793013002181>. doi:10.1016/j.compfluid.2013.05.023.
9. Lind, S., Xu, R., Stansby, P., Rogers, B.. Incompressible smoothed particle hydrodynamics for free-surface flows: A generalised diffusion-based algorithm for stability and validations for impulsive flows and

- propagating waves. *Journal of Computational Physics* 2012;231(4):1499 – 1523. doi:10.1016/j.jcp.2011.10.027.
10. Xu, R., Stansby, P., Laurence, D.. Accuracy and stability in incompressible SPH (ISPH) based on the projection method and a new approach. *Journal of computational Physics* 2009;228(18):6703–6725. doi:<https://doi.org/10.1016/j.jcp.2009.05.032>.
 11. Adami, S., Hu, X., Adams, N.. A transport-velocity formulation for smoothed particle hydrodynamics. *Journal of Computational Physics* 2013;241:292–307. doi:10.1016/j.jcp.2013.01.043.
 12. Colagrossi, A., Bouscasse, B., Antuono, M., Marrone, S.. Particle packing algorithm for SPH schemes. *Computer Physics Communications* 2012;183(8):1641–1653. doi:<https://doi.org/10.1016/j.cpc.2012.02.032>.
 13. Litvinov, S., Hu, X., Adams, N.. Towards consistence and convergence of conservative SPH approximations. *Journal of Computational Physics* 2015;301:394–401. URL: <https://linkinghub.elsevier.com/retrieve/pii/S0021999115005690>. doi:10.1016/j.jcp.2015.08.041.
 14. Dilts, G.A.. Moving-least-squares-particle hydrodynamics I: Consistency and stability. *International Journal for Numerical Methods in Engineering* 1999;44(8):1115–1155.
 15. Dilts, G.A.. Moving least-squares particle hydrodynamics II: conservation and boundaries. *International Journal for numerical methods in engineering* 2000;48(10):1503–1524.
 16. Bonet, J., Lok, T.S.. Variational and momentum preservation aspects of smooth particle hydrodynamic formulations. *Computer Methods in Applied Mechanics and Engineering* 1999;180(1):97 – 115. doi:10.1016/S0045-7825(99)00051-1.
 17. Frontiere, N., Raskin, C.D., Owen, J.M.. CRKSPH - a conservative reproducing kernel smoothed particle hydrodynamics scheme. *Journal of Computational Physics* 2017;332(1):160–209. doi:10.1016/j.jcp.2016.12.004.

18. Eitzlmayr, A., Koscher, G., Khinast, J.. A novel method for modeling of complex wall geometries in smoothed particle hydrodynamics. *Computer physics communications* 2014;185(10):2436–2448.
19. Chiron, L., De Lefte, M., Oger, G., Le Touzé, D.. Fast and accurate SPH modelling of 3d complex wall boundaries in viscous and non viscous flows. *Computer Physics Communications* 2019;234:93–111.
20. Marrone, S., Antuono, M., Colagrossi, A., Colicchio, G., Le Touzé, D., Graziani, G.. δ -SPH model for simulating violent impact flows. *Computer Methods in Applied Mechanics and Engineering* 2011;200:1526–1542. doi:10.1016/j.cma.2010.12.016.
21. Xiao, Y., Dong, H., Zhan, H., Gu, Y.. A new particle generation method for arbitrary 2D geometries in SPH modeling. *International Journal of Computational Methods* 2017;14(03):1750023. doi:<https://doi.org/10.1142/S0219876217500232>.
22. Domínguez, J., Crespo, A., Barreiro, A., Gómez-Gesteira, M., Mayrhofer, A.. Development of a new pre-processing tool for SPH models with complex geometries. In: *6th International SPHERIC workshop*. 2011:117–124.
23. Akinci, N., Cornelis, J., Akinci, G., Teschner, M.. Coupling elastic solids with smoothed particle hydrodynamics fluids. *Computer Animation and Virtual Worlds* 2013;24(3-4):195–203. doi:<https://doi.org/10.1002/cav.1499>.
24. Jiang, M., Zhou, Y., Wang, R., Southern, R., Zhang, J.J.. Blue noise sampling using an SPH-based method. *ACM Transactions on Graphics (TOG)* 2015;34(6):1–11. doi:<https://doi.org/10.1145/2816795.2818102>.
25. Ramachandran, P., Puri, K., Bhosale, A., Dinesh, A., Muta, A., Negi, P., Govind, R., Sanka, S., Pandey, P., Kaushik, C., et al. PySPH: a Python-based framework for smoothed particle hydrodynamics. *arXiv preprint arXiv:190904504* 2019;URL: <https://arxiv.org/abs/1909.04504>.
26. Ramachandran, P.. PySPH: a reproducible and high-performance framework for smoothed particle hydrodynamics. In: Benthall, S.,

- Rostrup, S., eds. *Proceedings of the 15th Python in Science Conference*. 2016:127 – 135.
27. Monaghan, J.J.. Simulating free surface flows with SPH. *Journal of Computational Physics* 1994;110:399–406.
 28. Wendland, H.. Piecewise polynomial, positive definite and compactly supported radial functions of minimal degree. *Advances in computational Mathematics* 1995;4(1):389–396.
 29. Adami, S., Hu, X., Adams, N.. A generalized wall boundary condition for smoothed particle hydrodynamics. *Journal of Computational Physics* 2012;231(21):7057–7075. doi:10.1016/j.jcp.2012.05.005.
 30. Negi, P., Ramachandran, P., Haftu, A.. An improved non-reflecting outlet boundary condition for weakly-compressible SPH. *Computer Methods in Applied Mechanics and Engineering* 2020;367:113119. doi:<https://doi.org/10.1016/j.cma.2020.113119>.
 31. Tafuni, A., Domínguez, J., Vacondio, R., Crespo, A.J.C.. A versatile algorithm for the treatment of open boundary conditions in smoothed particle hydrodynamics GPU models. *Computer methods in applied mechanical engineering* 2018;342:604–624. doi:10.1016/j.cma.2018.08.004.
 32. Dehnen, W., Aly, H.. Improving convergence in smoothed particle hydrodynamics simulations without pairing instability. *Monthly Notices of the Royal Astronomical Society* 2012;425(2):1068–1082. doi:10.1111/j.1365-2966.2012.21439.x.
 33. Swegle, J., Hicks, D., Attaway, S.. Smoothed particle hydrodynamics stability analysis. *Journal of computational physics* 1995;116(1):123–134. doi:<https://doi.org/10.1006/jcph.1995.1010>.
 34. Morris, J.P.. A study of the stability properties of sph. *arXiv preprint astro-ph/9503124* 1995;URL: <https://arxiv.org/abs/astro-ph/9503124>.
 35. Akinci, N., Akinci, G., Teschner, M.. Versatile surface tension and adhesion for SPH fluids. *ACM Transactions on Graphics (TOG)* 2013;32(6):1–8. doi:<https://doi.org/10.1145/2508363.2508395>.

36. Ramachandran, P.. automan: A python-based automation framework for numerical computing. *Computing in Science & Engineering* 2018;20(5):81–97. doi:10.1109/MCSE.2018.05329818.